Wideband linearly polarized transmitarray antenna for 60 GHz backhauling

Cyril Jouanlanne, Antonio Clemente, Mathieu Huchard, Julien Keignart, Cyril Barbier, Thierry Le Nadan, Laurent Petit

Wideband Linearly-Polarized Transmitarray Antenna for 60 GHz Backhauling

Cyril Jouanlanne, Antonio Clemente, *Member, IEEE*, Mathieu Huchard, Julien Keignart, Cyril Barbier, Thierry Le Nadan, Laurent Petit, *Member, IEEE*

***Abstract*—This communication presents the design of a linearly-polarized transmitarray antenna for backhauling applications at V-band (57 – 66 GHz). The antenna is composed of a planar circular-shape array with 1264 unit-cells printed on a three-metal layer standard PCB, an *ad-hoc* focal source, and a radome layer. A 3-bit phase resolution has been selected to achieve a gain higher than 31 dBi over the whole unlicensed 60 GHz-band and low side lobe levels. The presence of the radome near the array is taken into account in the unit-cell design. Experimental results are in line with the theoretical ones provided by an *in-house* CAD tool based on analytical model and electromagnetic simulations. The proposed design presents a measured broadside gain of 32.5 dBi at 61.5 GHz with an aperture efficiency of 42.7% and a wide 1-dB gain bandwidth of 15.4% (57 – 66.5 GHz).**

***Index Terms*—Transmitarray antenna, flat lens, discrete lens, backhauling, point-to-point communications, 5G, millimetre wave.**

I. Introduction

The rapid growth of mobile data traffic and the use of smartphone or other connected objects have recently drawn increased attention to the large amount of underutilized millimetre wave (mmWave) frequency bands (30 – 300 GHz) as a potential solution to achieve tens or hundreds of times more capacity compared to the current cellular networks. Recently, the Federal Communications Commission (FCC) examined the possibility of licensing the frequency band 24 – 90 GHz for use of fifth-generation (5G) mobile network services [1]. In this scenario, 5G wireless heterogeneous networks will be probably composed of medium-range macro-cells at sub-3 GHz bands, small-cells at sub-6 GHz, and small-cells at mmWave bands (28, 38, 60 GHz or E band 71 – 76 and 81 – 86 GHz) with a target peak capacity of 2 – 7 Gb/s near the access point [2],[3]. High-capacity (peak capacity around 10 – 25 Gb/s) mmWave backhaul links working in line-of-sight (LOS) conditions will also connect the access points to the core network [3],[4]. This high-capacity backhaul link offers operators multihop short- and medium-range links in the range of hundreds of meters to 1 km. Currently, three frequency bands are considered for mmWave backhauling: (i) the 28 GHz band, (ii) the V-band (57 – 66 GHz), and the (iii) E-band. In this paper, a fixed beam transmitarray antenna for backhauling at V-band is designed, optimized and characterized. In this frequency band, high-gain antennas (> 30 dBi) are required and a trade-off between the link budget, antenna cost and size should be considered [3].

Manuscript received February 26, 2016; revised November 8, 2016.

Cyril Jouanlanne, A. Clemente, and Julien Keignart are with CEA-LETI, F38054 Grenoble, France (e-mail: cyril.jouanlanne@cea.fr, antonio.clemente@cea.fr, julien.keignart@cea.fr).

Mathieu Huchard, Cyril Barbier, Thierry Le Nadan, and Laurent Petit are with Radiall, 38340 Voreppe, France (e-mail: mathieu.huchard@radiall.com, cyril.barbier@radiall.com, thierry.lenadan@radiall.com, laurent.petit@radiall.com).

Fig. 1. Exploded view of the complete transmitarray antenna.

Several antenna technologies such as parabolic reflectors, microstrip- [5], waveguide slot- [6],[7] and substrate-integrated waveguide [8],[9] (SIW)-based planar arrays, have been developed for wideband applications in the V-band requiring a gain > 30 dBi. A relatively complete survey on these technologies is presented in [7]. Thanks to their spatial feeding illumination, transmitarray antennas are very attractive if compared to microstrip-based arrays that suffer from large insertion loss at mmWaves. Furthermore, transmitarrays based on standard printed circuit board (PCB) technology are relatively low cost and efficient alternative solutions when compared to the parabolic reflector, SIW- and waveguide slot-based arrays. A transmitarray consists of one/or more focal sources [10]-[15] illuminating an array of unit-cells each one of them made of an *Rx* antenna coupled to a *Tx* antenna. The two antennas are connected by a phase-shifter in order to locally shift the transmission phase and focus the radiated beam in a desired direction. Electronically beam-scanning can be obtained by integrating in the array MEMS switches [16], p-i-n diodes [17], or varactors [18],[19].

The proposed linearly-polarized transmitarray (Fig. 1) uses a 3-bit phase quantization, which means a pool of eight unit-cells (called 0°, 45°, 90°, 135°, 180°, 225°, 270°, and 315°), to reach the required performances (maximum gain and SLL – Side Lobe Level) over the whole 57 – 66 GHz unlicensed band. This 3-bit unit-cell is based on two different architectures: (i) an optimized version of the simple patch unit-cell previously presented in [10] and (ii) a new capacitive fed patch architecture. The design is pushed to a Technology Readiness Level (TRL) corresponding to an industrial demonstrator. For instance, the focal source, including a profiled skirt protecting the antenna from its surroundings, is rather more complex than a standard pyramidal horn antenna usually used in the open literature for classical transmitarray antenna design. A polypropylene radome is also included to protect the array from its surrounding environment. It has been taken into account in the unit-cell design and optimization. The aperture phase

distribution and the illumination taper are optimized using the *in-house* software previously demonstrated [10],[14],[15] to obtain a radiation pattern in accordance with the required masks [20]. A wide 1-dB bandwidth of 15.4% (~57 – 66.5 GHz) and a relatively high aperture efficiency of 42.7% (directivity of the equivalent uniform aperture with a radius of 50 mm equal to 36.2 dBi at 61.5 GHz) are experimentally demonstrated.

The rest of the paper is organized as follows. The unit-cell and the focal source designs are presented in Section II and Section III, respectively. Then, the complete transmitarray design, simulation and measurement results are given in section IV. Finally, conclusions are drawn in Section V.

II. Unit-Cell Design and Frequency Response

Two different unit-cell architectures (*Type 1* and *Type 2*) are specifically designed for the considered transmitarray to reach a 3-bit phase resolution. The desired 45° relative phase-shift between each phase state is achieved using eight unit-cell configurations based on the two architectures. The 3-bit phase quantization is selected to make a trade-off between transmitarray quantization loss (< 0.3 dB if compared with a 360° phase-shift unit-cell), array radiation properties (SLL, etc.), and unit-cells bandwidth and complexity.

The unit-cells size is fixed to 2.5 × 2.5 mm² (i.e. 0.51λ × 0.51λ at the design frequency 61.5 GHz) and is composed of two patch antennas printed on the top and bottom layer of the dielectric structure (Fig. 2). A 17 µm-tick copper ground plane is printed on the inner layer and a metallized via-hole ensures the coupling between both patches. Several known design rules are used to achieve the 45° phase resolution such as *Tx* patch rotation, which induces a 180° phase-shift [10], patch resizing [21],[22] inducing in this case a phase-shift of 45°, and the use of two distinct unit-cell topologies (*Type 1* and *Type 2*) having an intrinsic 90° phase-shift [23].

A. 3-bits unit-cell design

The proposed unit-cell layout is based on a three-metal layer Printed Circuit Board (PCB) realized using two 508 µm-thick dielectric substrates with ε_r = 2.5 and tanδ = 0.0017. Firstly, the unit-cell *Type 1* is used to generate the phase states 0° and 45°. The 45° phase shift is obtained from the unit-cell with phase state 0° by resizing the geometrical parameters of the patches. In the same way, the unit-cell *Type 2* is used to achieve the phase states 90° and 135°. Starting from these four unit-cell phase states (0°, 45°, 90°, and 135°), the unit-cells with phase state 180°, 225°, 270°, and 315° have been respectively generated by physically rotating the upper patch with respect to the via-hole connection [10]. In order to reduce the coupling effects in the case of the 180°-rotation and to keep the aspect ratio of each unit-cells similar, a polarization shift of 90° is introduced between the *Rx* array and the *Tx* layers (90° rotation of each *Tx* patch). As a result, the transmitarray polarization is orthogonal to the incident wave coming from the focal source and, consequently, the spillover effects on the co-polar component of the transmitarray radiation pattern (SLL) could be reduced.

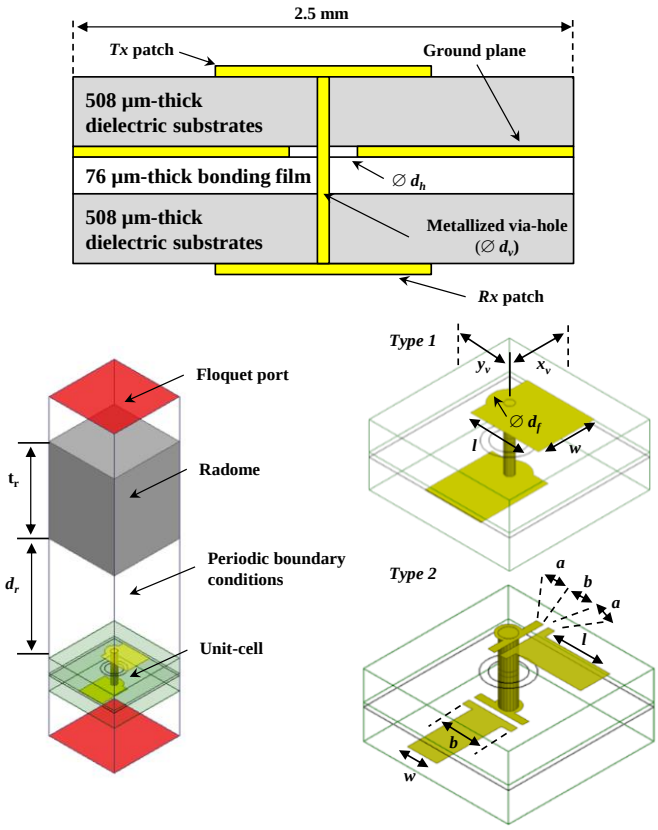

Fig. 2. Unit-cell cross-section view, architectures (*Type 1* and *Type 2*) and electromagnetic simulation setup including the radome.

Fig. 2 presents both unit-cell architectures as well as the simulation setup used to evaluate and optimize their performances. [0°, 45°, 180°, 225°] unit-cell designs (*Type 1*) are similar to the one presented in [10] (an optimization has been done to increase the bandwidth) and [90°, 135°, 270°, 315°] unit-cell designs (*Type 2*) are based on the capacitive fed patch architecture. All the unit-cell physical dimensions are provided in Table I. Each unit-cell state is optimized using the commercial electromagnetic simulation software Ansys HFSS. In order to study the unit-cell behavior when an infinite array geometry is considered, the full-wave simulations are performed using Floquet ports and periodic boundary conditions. The radome distance from the unit-cell defined at the array center (d_r = 4 mm) and its thickness (t_r = 3.2 mm) are simultaneously optimized with the unit-cell parameters to obtain, for each unit-cell, a reflection coefficient lower than -10 dB, low insertion loss (< 1 dB), and the desired 45° phase resolution on the full unlicensed V-band (57 – 66 GHz). Since the fabricated radome has a non-flat shape to increase its mechanical resistance, the unit-cell performance is studied considering a variation of the distance d_r in the range 3.5 - 4 mm. For the worst case scenario, a maximum transmission phase variation between –2.3° and 4.1° is achieved when compared to the case of nominal distance (d_r = 4 mm). On the other side, the insertion loss variation is equal to ±0.5 dB; hence, in the transmitarray optimization and simulation process, only the nominal responses of unit-cells are used.

B. 3-bits unit-cell frequency response

The 3-bit unit-cell simulated reflection coefficients, calculated under normal incidence and presented in Fig. 3(a), are lower than -9.65 dB for each unit-cell over the whole 57 – 66 GHz band. Thanks to the low unit-cell reflection coefficient, the transmitarray reflection losses could be minimized reducing the ripple inside the proposed tapered focal source, which could cause distortions on the transmitarray radiation pattern. Furthermore, the simulated transmission coefficient, computed under normal incidence, remains better than -1dB (Fig. 3(b)) for each unit-cell state on the whole band of interest.

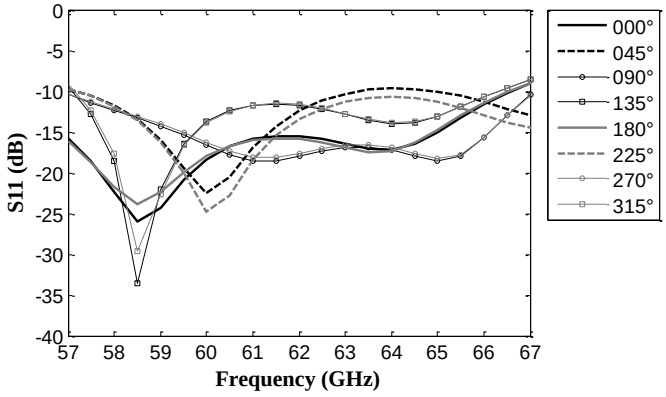

(a)

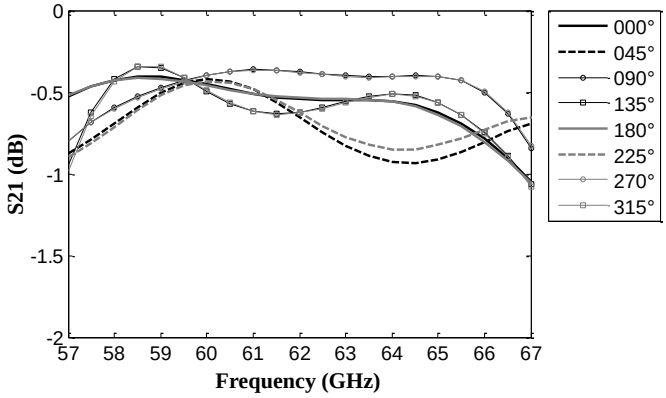

(b)

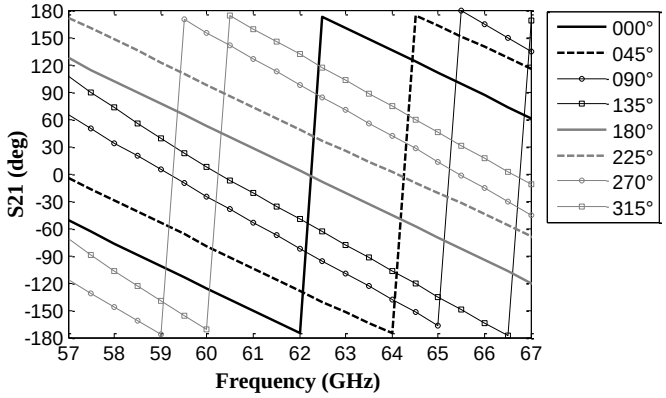

(c)

Fig. 3. 3-bit unit-cell simulated frequency response computed under normal incidence. (a) Amplitude of the reflection coefficient, (b) amplitude of the transmission coefficient, and (c) transmission phase.

Finally, the simulated unit-cell transmission phase is presented in Fig. 3(c). The unit-cells have been optimized to have a phase-shift of 45° between each unit-cell phase state and obtain a 3-bit phase quantization. In addition, under oblique incidence, the unit-cell transmission coefficients and transmission phases are very stable up to 40° as in the case of [17],[22]; hence, in the transmitarray design, only normal incidence responses are used to optimize its final phase distribution and geometry.

TABLE I
MAIN UNIT-CELL (UC) GEOMETRIC PARAMETERS

UC	l	w	a	b	x_v	y_v	d_v	d_h	d_f
0°	1.20	1.00	-	-	0.99	0.99	0.15	0.75	0.60
45°	1.00	0.87	-	-	1.01	1.01	0.20	0.75	0.52
90°	1.11	0.50	0.11	0.09	0.71	0.71	0.25	0.72	-
135°	1.05	0.50	0.11	0.09	0.71	0.71	0.20	0.72	-

* All the parameters are expressed in *mm*.

III. FOCAL SOURCE DESIGN

In this section, the design, simulation, fabrication and characterization of the proposed *ad-hoc* linearly-polarized focal source is discussed. In most of the works published in the open literature, the transmitarray is placed in the free space and illuminated by a standard horn antenna. However, in a real industrial product, several additional constraints must be taken into account: (i) shield the region between the focal source and the lens from the surrounding environment; (ii) provide the mechanical robustness for integration into an outdoor unit (ODU); and (iii) reduce as much as possible the depth between the focal point and the lens. From the electrical point of view, the focal source must be designed to shape the electric field distribution in the plane of the lens with amplitude approximating a Gaussian distribution and phase approximating a spherical wave front. Furthermore, the illumination taper must be optimized to obtain the best trade-off between the array bandwidth, the spillover, the aperture efficiency, and the focal distance. The aperture taper has also an impact on the ripples caused by the waves backward reflected by the planar lens inside the *ad-hoc* focal source cavity. The cross-polar pattern radiated by the focal source has also been minimized.

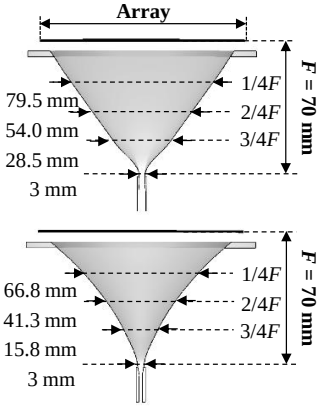

Fig. 4. Pictures of the fabricated focal source.

The realized *ad-hoc* focal source made in plastic injection technology and electroplated with nickel over copper is shown in Fig. 4. Its design geometry was optimized by taking into account in the electromagnetic simulation the screw holes, the mechanical elements required for fixture and the plastic injection constraints. The radiating element is a tapered waveguide section having a standard WR-15 rectangular waveguide aperture on the input interface and a smaller square aperture (3×3 mm²) on the radiating side. The shape and size of this square section have a strong influence on the shape of the focal source radiation pattern and its directivity. According to the diffraction theory, the far-field radiated by an aperture is given by the Fourier transform of the aperture, thus a rectangular aperture gives a distribution close to a *cardinal sine* function (or *sinc* function) in the far-field (or in the lens plane). The smaller is the aperture, the wider is the amplitude distribution. In our case, the size was chosen to obtain a similar beamwidth in the E- and H-planes with a maximum directivity of 15 dBi. The square aperture is tapered through three successive elliptical sections (details presented in Fig. 4) into the final circular aperture having a diameter of 105 mm and located 5 mm away from the transmitarray plane. The distance between the square primary aperture and the array plane is equal to 70 mm. Finally, the profiles from the squared primary section to the final circular aperture are modeled by spline lines and have been optimized to minimize the ripple in the array plane.

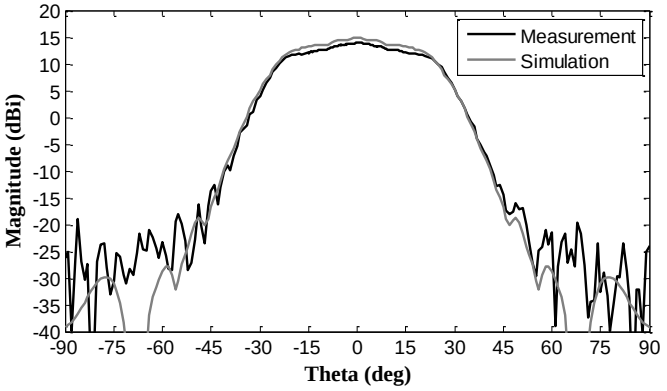

(a)

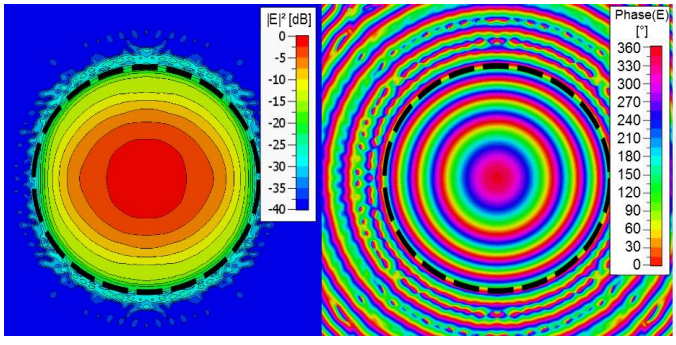

(b)

Fig. 5. Focal source performances at 62 GHz. (a) Measured and simulated radiation pattern on the E-plane. (b) Simulated amplitude and phase of the incident electric field computed on the array aperture.

The simulated and measured radiation patterns (E-plane) computed at 62 GHz are presented in Fig. 5(a). A maximum gain of 14.1 dBi has been measured in acceptable agreement with the simulated one, which is equal to 14.9 dBi. Since the focal source aperture is very close to the array plane (5 mm, i.e 1 wavelength at 60 GHz), its simulated radiated field has been analyzed as a function of the distance. The simulated electric field distribution (amplitude and phase) calculated on the array plane is depicted in Fig. 5(b).

IV. Linearly-Polarized Transmitarray: Design and Characterization

In this section, the linearly-polarized transmitarray working in the V-band and its experimental characterization are presented. Our objective was to obtain a gain > 31 dBi (required to guarantee a coverage of 100 – 200 m in the 60 GHz-band), ensure a maximum gain as stable as possible on the full-unlicensed V-band, and obtain a relatively compact structure (e.g. focal distance F and array thickness).

A. Transmitarray design and optimization

The linearly-polarized transmitarray is optimized and simulated using an *in-house* CAD tool developed at CEA-LETI [10] and previously validated at X- [17], Ka- [14] and V-band [10]. Using analytical formulas and the results of the unit-cell and focal source electromagnetic simulations (radiation pattern, scattering matrix, etc.), the software extracts the transmitarray behavior (frequency response and radiation pattern) as well as the optimal phase distribution. The analysis and optimization can be easily computed as a function of the transmitarray parameters such as the array geometry and size, the number of unit-cell, the focal distance, etc.

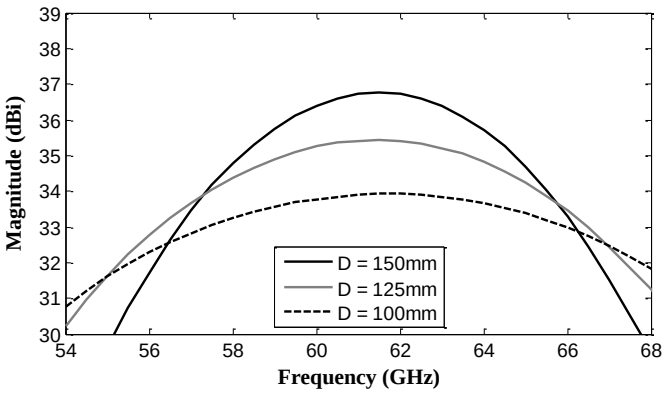

Fig. 6. Transmitarray frequency response computed as a function of the array diameter (focal distance 70 mm) using the theoretical focal source and unit-cells described in [15].

To estimate the impact of the array size on the transmitarray 1-dB bandwidth, a preliminary analysis has been carried out using the *in-house* simulation tool. This study is performed considering a theoretical 3-bit unit-cell and a theoretical focal source ($cos^n\theta$) [15] with radiation performances (directivity and beamwidth) similar to the proposed focal source presented in Section III. The focal distance, which has been optimized in the pre-design phase, is fixed to 70 mm.

The simulated transmitarray frequency response computed for three different array diameters (D) and optimizing the phase

distribution on the array aperture to achieve the maximum gain is presented in Fig. 6. In the figure, it can be observed that by reducing the array diameter with constant focal source directivity and *F*, the maximum gain is reduced as expected but the transmitarray frequency response is flattened with a very stable gain in the band 57 – 66 GHz. This phenomenon is due to phase-shift behavior of the unit-cell (almost constant on the frequency band) and the phase compensation, which is calculated at the central frequency 61.5 GHz. In fact, in this case, the phase error, which is defined as the difference between the fixed phase compensation calculated at the central frequency and the necessary phase compensation distribution calculated at a frequency different from the optimization one, increases away from the optimization frequency and causes a reduction of the gain. Techniques based on the true-time-delay correction could be used to reduce this bandwidth issue as demonstrated in [24] at the cost of a more complex and expensive (increased number of layers and substrates) unit-cell and array architecture.

B. Fabricated transmitarray and experimental results

The fabricated 100 mm-diameter (40 unit-cells on the vertical and horizontal axes) linearly-polarized transmitarray based on the proposed 3-bit unit-cells and focal source is presented in Fig. 7. It has been realized using standard PCB laminating techniques and characterized in the CEA-LETI anechoic chamber (20 m length × 12 m width × 12 m height Fig. 7(b)).

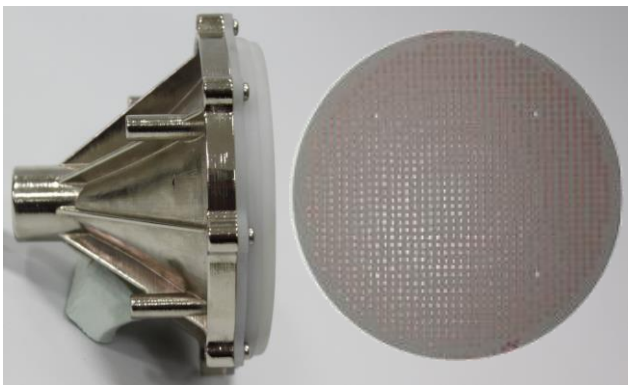

(a)

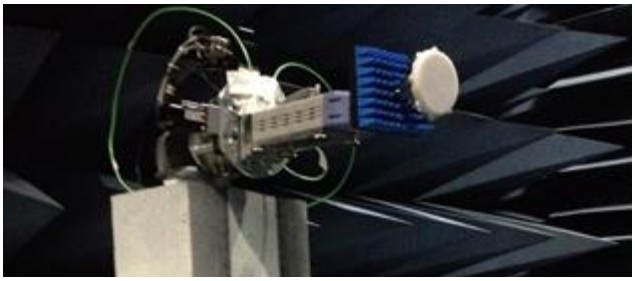

(b)

Fig. 7. Fabricated linearly-polarized transmitarray. (a) Picture of fabricated array. (b) Picture of the transmitarray in the anechoic chamber during the measurement.

The antenna maximum gain measured in the broadside direction as a function of the frequency is plotted in Fig. 8 and is compared to the simulated results computed using the *in-house* transmitarray optimization tool. A maximum gain of 32.5 dBi has been obtained with a wide 1-dB bandwidth of 15.4% (~57–66.5 GHz) and an aperture efficiency of 42.7%. Instead, the simulated maximum gain is equal to 31.8 dBi. The difference between the simulated and measured results is probably due to: (i) the unit-cell simulation performed for each phase-state considering an infinite array of identical elements; (ii) the use in the transmitarrays simulation of the *ad-hoc* focal source simulated far-field; and (iii) the non-constant distance between the radome and the planar array (mechanical constraint) not taken into account in the unit-cell simulations.

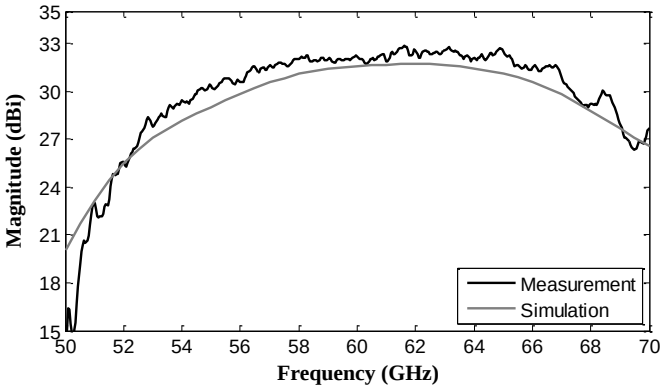

Fig. 8. Measured and simulated broadside gains with respect to the frequency.

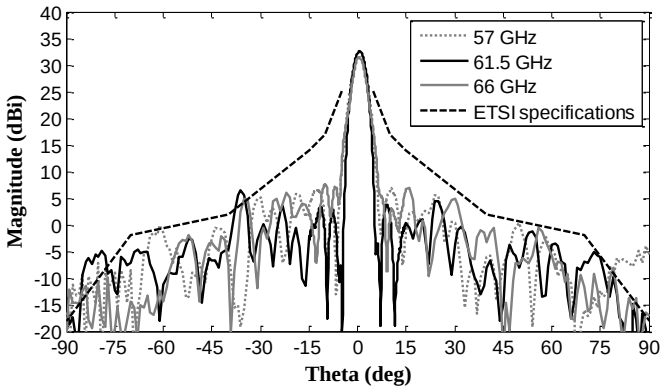

(a)

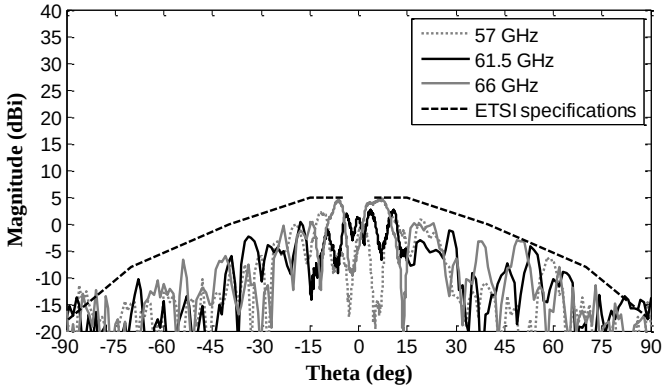

(b)

Fig. 9. Measured gain radiation pattern, (a) co- and (b) cross-polar components, of the linearly-polarized transmitarray in the H-plane at 57, 61.5, and 66 GHz. The patterns are compared to ETSI point-to-point communication requirements [20].

The measured co- and cross-polar gain radiation pattern (H-plane) at three different frequencies (57, 61.5, and 66 GHz) are presented in Fig. 9 and compared to the ETSI requirements for point-to-point equipment and antennas [20]. A cross-polarization discrimination (XPD) higher than 31 dB has also been demonstrated on the whole operating band. Similar results have been obtained on the E-plane.

The main performances (gain, aperture efficiency, and 1-dB gain bandwidth) of the proposed transmitarray are presented in Table II and compared with the performances of the recent structures presented in the open literature [11]-[13] and with previous demonstration presented by our group [10].

TABLE II
COMPARISON OF THE CURRENT RESULTS WITH RECENTLY PUBLISHED WORKS

	Freq. (GHz)	**Gain (dBi)**	ϵ_{ap} **(%)**	**1-dB gain BW (%)**
[11]	10.3	24.8	55	15.5
[12] – (1)	13.5	30.2	50	9.8
[12] – (2)	13.5	29.9	47	11.7
[13]	30.3	28.6	35.6	7.5
[10]	60	23.9	12.9	7.6
This work	61.5	32.5	42.7	15.4

V. CONCLUSIONS

A linearly-polarized 1264-element transmitarray working in the V-band has been designed and experimentally characterized. The dimensions of the planar array have been optimized to reach an almost flat response over the whole band (57 - 66 GHz) and obtain a relative compact architecture. A trade-off between array size, aperture efficiency, and focal distance is done to guarantee the bandwidth, pattern, and compactness requirements. The designed transmitarray is circular with a diameter of 100 mm and is based on a 3-bit unit-cell (45° phase resolution on the array aperture). The 3-bit phase resolution is selected to obtain optimal performances in terms of gain, radiation pattern mask and bandwidth, and reduce the complexity of the unit-cell. A profiled focal source has been specifically designed providing an optimized illumination of the transmitarray as well as a space shielding between the horn and the lens from the surrounding.

The proposed design presents a measured broadside gain of 32.5 dBi at 61.5 GHz with an aperture efficiency of 42.7% and a 1-dB gain fractional bandwidth of 15.4% (57 – 66.5 GHz). Good agreement with the numerical results has been demonstrated.

REFERENCES

[1] FCC, "Notice of inquire 14-154," Oct. 2014.

[2] T. S. Rappaport, S. Sun, R. Mayzus, H. Zhao, Y. Azar, K. Wang, G. N. Wong, J. K. Schulz, M. Samimi, and F. Gutierrez, "Millimeter wave mobile communications for 5G cellular: it will work!," *IEEE Access*, vol. 1, pp. 335-349, 2013.

[3] C. Dehos, J. L. González, A. De Domenico, D. Kténas, and L. Dussopt, "Millimeter-wave access and backhauling: the solution to the exponential data traffic increase in 5G mobile communications systems?," *IEEE Commun. Mag.*, vol. 52, no. 9, pp. 88-95, Sep. 2014.

[4] M. Shariat, M. Dianati, K. Seppanen, T. Suihko, J. Putkonen, and V. Frascolla, "Enabling wireless backhauling for next generation mmWave networks", in *Proc. 2015 European Conf. Net. Commun.* (*EuCNC*) pp. 164-168, Jul. 2015.

[5] M. Li and K.-M. Luk, "Low-cost wideband microstrip antenna array for 60-GHz applications," *IEEE Trans. Antennas Propag.*, vol. 62, no. 6, pp. 3012–3018, Jun. 2014.

[6] G.-L. Huang, S.-G. Zhou, T.-H. Chio, H.-T. Hui, and T.-S. Yeo, "A low profile and low sidelobe wideband slot antenna array fed by an amplitude-tapering waveguide feed-network," *IEEE Trans. Antennas Progag.*, vol. 63, no. 1, pp. 419–423, Jan. 2015.

[7] D. Zarifi, A. Farahbakhsh, A. U. Zaman, and P.-S Kildal, "Design and fabrication of a high-gain 60-GHz corrugated slot antenna array with ridge gap waveguide distribution layer," *IEEE Trans. Antennas Progag.*, vol. 64, no. 7, pp. 2905–2913, Jul. 2016.

[8] J. Wu, Y. J. Cheng, and Y. Fan, "A wideband high-gain high-efficiency hybrid integrated plate array antenna for V-band inter-satellite links," *IEEE Trans. Antennas Propag.*, vol. 63, no. 4, pp. 1225–1233, Apr. 2015.

[9] Y. Li and K.-M. Luk, "60-GHz substrate integrated waveguide fed cavity-backed aperture-coupled microstrip patch antenna arrays," *IEEE Trans. Antennas Propag.*, vol. 63, no. 3, pp. 1075–1085, Mar. 2015.

[10] H. Kaouach, L. Dussopt, J. Lantéri, R. Sauleau, and Th. Koleck, "Wideband low-loss linear and circular polarization transmit-array in V-band," *IEEE Trans. Antennas Propag.*, vol. 59, no. 7, pp. 2513-2523, Jul. 2011.

[11] B. Rahmati and H. R. Hassani, "High efficient wideband slot transmitarray antenna," *IEEE Trans. Antennas Propag.*, vol. 63, no. 11, pp. 5149-5155, Nov. 2015.

[12] A. H. Abdelrahman, P. Nayeri, A. Z. Elsherbeni, and F. Yang, "Bandwidth improvement methods of transmitarray antennas," *IEEE Trans. Antennas Propag.*, vol. 63, no. 7, pp. 2946-2954, July 2015.

[13] C. G. M. Ryan, M. R. Chaharmir, J. Shaker, J. R. Bray, Y. M. M. Antar, and A. Ittipiboon, "A wideband transmitarray using dual-resonant double square rings," *IEEE Trans. Antennas Propag.*, vol. 58, no. 5, pp. 1486–1493, May 2010.

[14] L. Di Palma, A. Clemente, L. Dussopt, R. Sauleau, P. Potier, P. Pouliguen "Circularly-polarized transmitarray with sequential rotation in Ka-band," *IEEE Trans. Antennas Propag.*, vol. 63, no. 11, pp. 5118-5124, Nov. 2015.

[15] A. Clemente, L. Dussopt, R. Sauleau, P. Potier, and P. Pouliguen, "Focal distance reduction of transmit-array antennas using multiple feeds," *IEEE Antennas Wireless Propag. Lett.*, vol. 11, pp. 1311–1314, Nov. 2012.

[16] C. Chih-Chieh, B. Lakshminarayanan, and A. Abbaspour-Tamijani, "A programmable lens-array antenna with monolithically integrated MEMS switches," *IEEE Trans. Microw. Theory Tech.*, vol. 7, no. 8, pp.1874–1884, Aug. 2009.

[17] A. Clemente, L. Dussopt, R. Sauleau, P. Potier, and P. Pouliguen, "Wideband 400-element electronically reconfigurable transmitarray in X band," *IEEE Trans. Antennas Propag.*, vol. 61, no. 10, pp. 5017-5027, Oct. 2013.

[18] L. Boccia, I. Russo, G. Amendola, and G. Di Massa, "Multilayer antenna-filter antenna for beam-steering transmit-array applications," *IEEE Trans. Microw. Theory Tech.*, vol. 60, no. 7, pp. 2287–2300, Jul. 2012.

[19] J. Y. Lau and S. V. Hum, "A wideband reconfigurable transmitarray element," *IEEE Trans. Antennas Propag.*, vol. 60, no. 3, pp. 1303–1311, Mar. 2012.

[20] ETSI EN 302 217-4-2 V1.5.1 (2010-01)

[21] W. An, S. Xu, and F. Yang, "A two-layer transmitarray antenna," in *Proc. IEEE Antennas Propag. Soc. Int. Symp.*, Memphis, TN, Jul. 2014, pp. 864-865.

[22] K. Pham, N. T. Nguyen, A. Clemente, L. Di Palma, L. Le Coq, L. Dussopt, and R. Sauleau, "Design of wideband dual lineraly-polarized transmitarray antennas," *IEEE Trans. Antennas Propag.*, in press.

[23] A. Abbaspour-Tamijani, K. Sarabandi, and G. M. Rebeiz, "A millimetre-wave bandpass filter-lens array," *IET Microw., Antennas & Propag.*, vol. 1, no. 2, pp. 388_395, Apr. 2007.

[24] M. Li, and N. Behdad, "Wideband true-time-delay microwave lenses based on metallo-dielectric and all-dielectric lowpass frequency selective surfaces," *IEEE Trans. Antennas Propag.*, vol. 61, no. 8, pp. 4109-4119, Aug. 2013.